DOI 10.4430/bgo00427

Comparative accuracy analysis of DEMs generated from descending and ascending orbit TerraSAR-X data

H.B. Makineci

Geomatics Engineering Department, Konya Technical University, Selçuklu, Konya, Turkey

(Received: 21 February 2023; accepted: 28 May 2023; published online: 27 July 2023)

ABSTRACT Determining the terrain structure of the Earth, a dynamic planet, creating a Digital Elevation Model (DEM) of some parts, and keeping them up to date, are basic necessities for human beings. In this research, DEMs produced using ascending (TRXASC) and descending (TRXDSC) orbit data pairs obtained from the current TerraSAR-X satellite data, and Terra World (TW) DEM (created with the help of data acquired by TanDEM-X), were subjected to point-based accuracy analysis. Standard deviations of the grid point elevation values were calculated using 43,750 digitally-produced grid points, within the study area (5.5×8.5 km^2), using different statistical methods. For the accuracy analysis, a 5-metre resolution DEM, created from the aerial photogrammetry technique of the national authority, General Directorate of Mapping (HGM), was used as the DEM basemap. Grid points are also examined according to two basic classes (slope classes and CORINE classes). The deficiency of prior studies using CORINE classes in this context, the preference for segmented-multiple subclasses used for slope classes, and the re-accuracy analysis of all statistical analyses, eliminating the gross error points, significantly contributed to the research with original findings.

Key words: ascending and descending TerraSAR data, CORINE, TanDEM-X world DEM, statistical accuracy analysis.

1. Introduction

The model, in which elevation information of any region on the Earth's surface is represented in the digital environment and raw data are presented spatially, is called the Digital Elevation Model (DEM). Over the last half century, DEMs, free of regional influences and containing the highest accuracy data, have been globally produced and continue to be created by many manufacturers worldwide (Zhang and Montgomery, 1994; Mukherjee *et al*., 2013; Balasubramanian, 2017). Since the DEM is an essential source of information, current DEMs that promise high accuracy in volume calculation, deformation research, generation of urban development models, different simulations, and, finally, meta-universes are preferred as basemaps (Akturk and Altunel, 2019; Rocha *et al*., 2020; Muthusamy *et al*., 2021; Ibrahim, 2023). Depending on the terrain, different DEM sources provide different accuracies in other parts of the world (Mukherjee *et al*., 2013; Polidori and El Hage, 2020; Li *et al*., 2022; El-Quilish *et al*., 2023).

Since it is impossible to create a one-to-one DEM by surveying the entire Earth surface and DEM accuracy is of great importance for end users, interpolation methods based on different mathematical models are used in DEM creation (Salekin *et al*., 2018; Habib *et al*., 2020; Huqqani

et al., 2022). While interpolation methods can generally deliver higher accuracy results in rather flat rural areas, like deserts, plains, etc., they may be insufficient in steep rocky areas, dense urban areas, and areas with significantly refracted terrain, where there are sudden changes in slope. In addition to using interpolation methods to create non-discontinuous DEMs, remote sensing sensors are frequently used to obtain world models. Remote sensing is the most accepted method for obtaining DEM data of large areas, cities, regions, countries, and even of the entire world, in a relatively short time and with high accuracy (Liu *et al*., 1999; Chen *et al*., 2016; Atkinson *et al*., 2022).

Compared to optical remote sensing sensors, RADAR sensor systems can obtain elevation information on objects with higher accuracy and more easily (Hilton *et al*., 2003; Rabus *et al*., 2003; Nardò *et al*., 2020). Synthetic Aperture Radar (SAR) systems are mostly used as a modern DEM generation approach. DEM is an indispensable primary product in interferometric SAR (InSAR) research. In InSAR studies, positive developments are experienced in DEM creation with increasing spatial resolution in sensing sensors. It is observed that different SAR sensors, that have emerged in recent years, provide significant vertical accuracy increases in DEM creation compared to DEMs obtained with previous sensors (Shabou *et al*., 2012; Makineci and Karabörk, 2016; Chu and Lindenschmidt, 2017; Luo *et al*., 2020; Zhang *et al*., 2023).

The Shuttle Radar Topography Mission (SRTM), globally the most well-known DEM, as a result of its mission completed in February 2000, is a global free-of-charge DEM with a spatial resolution of 3 arcseconds and 1 arcsecond (90 m and 30 m), which has collected data between 60° north and 60° south latitudes, and continues to deliver. Famous DEM sources such as SRTM, the Advanced Spaceborne Thermal Emission and Reflection Radiometer Global Digital Elevation Model (ASTER GDEM), and the ALOS Global Digital Surface Model "ALOS World 3D - 30m" (AW3D30), are data sets with a horizontal resolution of approximately 30-metre mesh (1 arcsecond), and are widely used by researchers (Mukherjee *et al*., 2013; Schellekens *et al*., 2014; Bayburt *et al*., 2017; Courty *et al*., 2019; Nardò *et al*., 2020; Chymyrov, 2021; Li *et al*., 2022). Keeping DEM sources up to date is an as essential preference factor as spatial resolution since the Earth's surface is not stable and is constantly changing (due to human or natural causes). Especially recently, an up-to-date and high spatial resolution DEM has been obtained using high-resolution X-band SAR data with a wavelength range of 2.4 to 3.75 cm acquired from TerraSAR-X and TanDEM-X satellites. In addition, the TanDEM-X mission global DEM, obtained between 2010 and 2015, has a spatial resolution of 0.4 arcseconds (Erten *et al*., 2018). The Terra World DEM (TWDEM) has a 12-metre spatial resolution at the equator (Collins *et al*., 2015; Becek *et al*., 2016; Altunel, 2019; Farooq *et al*., 2019; Mason *et al*., 2021). Researchers have used TWDEM, which offers higher spatial resolution (in terms of elevation) and more up-to-date data, as a basemap DEM in many critical studies. According to the accuracy analysis results obtained, it has been shown to give high spatial accuracy in different terrain groups. Analyses, through statistical methods, determine the differences between the models and accuracy (Farooq *et al*., 2019; Gümüs *et al*., 2021; Torun and Orhan, 2021; Torun, 2022).

Accuracy analyses are performed by classifying the land according to the terrain structure, editing if needed, and comparing the differences between the DEMs created and a high-accuracy DEM. This method can provide detailed information about the elevation accuracy of the created DEMs. In addition, with this comparison, it is possible to minimise the errors caused by different interpolation techniques used in DEM production. By dividing the accuracy analysis into sub-small equal parts (grid), the minimum (*min*), maximum (*max*), mean (*mean*), median (*med*), standard deviation (*SD*), and root-mean-square error (*RMSE*) values can be calculated according to the differences of the grid points. Finding and analysing the results is the most characteristic type of

analysis in general accuracy research. Error sources can be eliminated in the standard distribution one-sigma, two-sigma, and three-sigma regions with the three-sigma rule, which minimises the factors affecting accuracy (Polidori and El Hage, 2020; Di Lascio *et al*., 2022; Gelfand, 2022). For land classification, details created from DEMs, such as slope, aspect, and hillshade, or regional classifiers, such as Coordination of Information on the Environment (CORINE), are preferred (Balzter *et al*., 2015; Tayebi *et al*., 2017; Kumar *et al*., 2019; Basu, 2021; El-Quilish *et al*., 2023). Thus, statistical analysis results can reveal the accuracy of the product realised in parts rather than presenting the general framework. The lack of a point elevation accuracy assessment research for CORINE classes, belonging to different areas, results in a gap in the literature on this subject.

The data collection technique of SAR satellites causes geometrically different results for ascending and descending orbits. For this reason, different elevation products are obtained during data acquisition. As a result, satellite data belonging to different orbits were selected and compared in order to increase the reliability of the accuracy analysis. In this study, the elevational accuracy of the TRXDSC and TRXASC DEMs (obtained by separately using the TerraSAR-X satellite data pair with the descending orbit and the TerraSAR-X satellite data pair with the ascending orbit), and the TWDEM (produced with the TanDEM-X), were analysed in the specific study area. Orthomosaic maps, created from images taken by CCD (charged-coupled device) cameras with the photogrammetric technique (sourced from ground control points and operator-supported Key Point-Tie Point creation), were submitted to national institutions by the General Directorate of Maps (GDM, locally known as HGM) (Cosandier, 1999; Graham *et al*., 2019; Amami *et al*., 2022; Śledź and Ewertowski, 2022). The DEM created for orthorectification (HGMDEM) was used in accuracy analysis with its spatial resolution (5 m) (Konya *et al*., 2018; Yildiz *et a*l., 2018). The study area (approximately 47 km^2) was divided into grids, and equal grids were produced (Zhang and Montgomery, 1994). Statistical analyses, made from the points in the centre of the 43,750 grids produced, were performed as *min*, *max*, *mean*, *med*, *SD*, and *RMSE*. Then, 43,750 points were divided into seven different slope classes (0-2°, 2-5°, 5-8°, 8-17°, 17-24°, 24-33°, and 33-67°). According to the classification made with CORINE, nine different land classes are represented in the study area. While performing statistical accuracy analyses, an additional analysis was carried out according to the 95% confidence interval of the standard distribution. In the accuracy analysis performed with all 43,750 grid points, the *RMSE* value between TWDEM and HGMDEM was determined as 1.47 m. When this value is examined for points outside the 95% confidence interval, it has been calculated to be around 1.05 m, increasing with an accuracy of approximately 42 cm.

As a result of the research, the *RMSE* value of the differences for the two DEMs produced was 4.31 m for TRXASC-HGMDEM and 5.28 m for TRXDSC-HGMDEM. According to the literature, it can be said that the accuracy of the DEMs produced for this area, where the mountainous lands and the average slopes are high, are also acceptable (Lee *et al*., 1988; Eckert *et al*., 2005; Wu *et al*., 2008; Das *et al*., 2016; Makineci and Karabörk, 2016; Alvioli *et al*., 2020; Gdulová *et al*., 2020; Chymyrov, 2021; Karabörk *et al*., 2021). Statistical analyses of all grid points with slope angles between 2° and 5° have been determined as the region with the highest accuracy of the produced DEMs and ready-to-use TWDEMs. Another output of the study confirms that the DEMs created from the ascending orbit data pair always show higher accuracy than the DEMs created from the descending orbit data pair in this study area. Statistical analyses of all grid points for CORINE classes, which identify land principally occupied by agriculture, with significant areas of natural vegetation and non-irrigated arable land areas, has the highest accuracy with 0.88 m and 0.84 m *RMSE* values, respectively. When these values are examined for points outside the 95% confidence interval, they show an increase in accuracy of approximately 10 cm, and are calculated around 0.74 m and 0.77 m, respectively, for land principally occupied by agriculture,

with significant areas of natural vegetation and non-irrigated arable land areas. In this research, based on a slope-CORINE classification (never before adopted in accuracy assessments of DEM studies), an analysis of the differences of the grid points, within the 95% confidence interval, was performed. The elevation accuracies of both CORINE classes and slope classes are discussed and presented for the reader's attention. Using TerraSAR-X satellite data, it is possible to say, according to the literature, that no other research has been conducted yet on comparing DEM accuracies with CORINE classes in this context. For this reason, the research is both a pioneer and original research.

2. Materials and methods

2.1. Study area and grid points

The study area, located in the Selçuklu district in Turkey between 32°24'30'' and 32°27'55'' E longitude and 37°55'20'' and 37°59'25'' N latitude, NW of Konya city centre, covers an area of 5.5×8.5 km^2 (approximately 47 km^2) in terms of surface area. The selected area is (mainly) a region with a plateau-like terrain, where no DEM has been manually produced (with terrestrial survey) before. Pixel-based work in the working area is impossible due to the size of the area and the inadequacy of the computer hardware. For this reason, grids representing the area were created approximately every 30 m and pictured by placing a point in the centre. A total of 43,750 grid points were produced by 175 points along the 5.5-kilometre line, and 250 points along the 8.5-kilometre line. The grid points generated were used for statistical analysis, and slope information of the land was used for land classification. Thus, analyses were carried out according to the specific features of the grid points. Fig. 1 shows the boundaries of the study area, the locations of the grid points, and the general slope structure of the land.

As seen in Fig. 1a, the land has been classified according to seven different slope classes: 0-2° flattest areas, 2-5° flat areas, 5-8° slightly sloping areas, 8-17° less sloping areas, 17-24° sloping areas, 24-33° steep slope areas, and 33-67° the steepest slope areas. The mean slope of 43,750 identified points is 12.3° and the *SD* value was determined as 7.7°.

2.2. HGMDEM data

None of the DEMs used were created by reading one-to-one points from the field. DEMs created by remote sensing and photogrammetry techniques are based on mathematical operations as office production, so that there are fewer or even no field processes. For example, the DEM and HGMDEM (offering the highest spatial accuracy in this research) were produced by means of automatic mapping (starting from stereo aerial photographs, covering all the details of the land topography, including man-made features and vegetation), with a 5-metre grid spacing and 90% confidence interval (LE90), and the elevation data resulted in a vertical accuracy of ±3 m, after removing the gross errors. Level-0 DEM5 was produced in all areas where aerial photographs were taken, with uncorrected gross errors and water surfaces (sea, lake, and broad-bed creek).

2.3. TERRAWORLD DEM data

With the 12-metre spatial resolution data and within the scope of TanDEM-X High-Resolution Elevation Exchange-TREx, Terra World DEM created digital elevation, covering all the details of

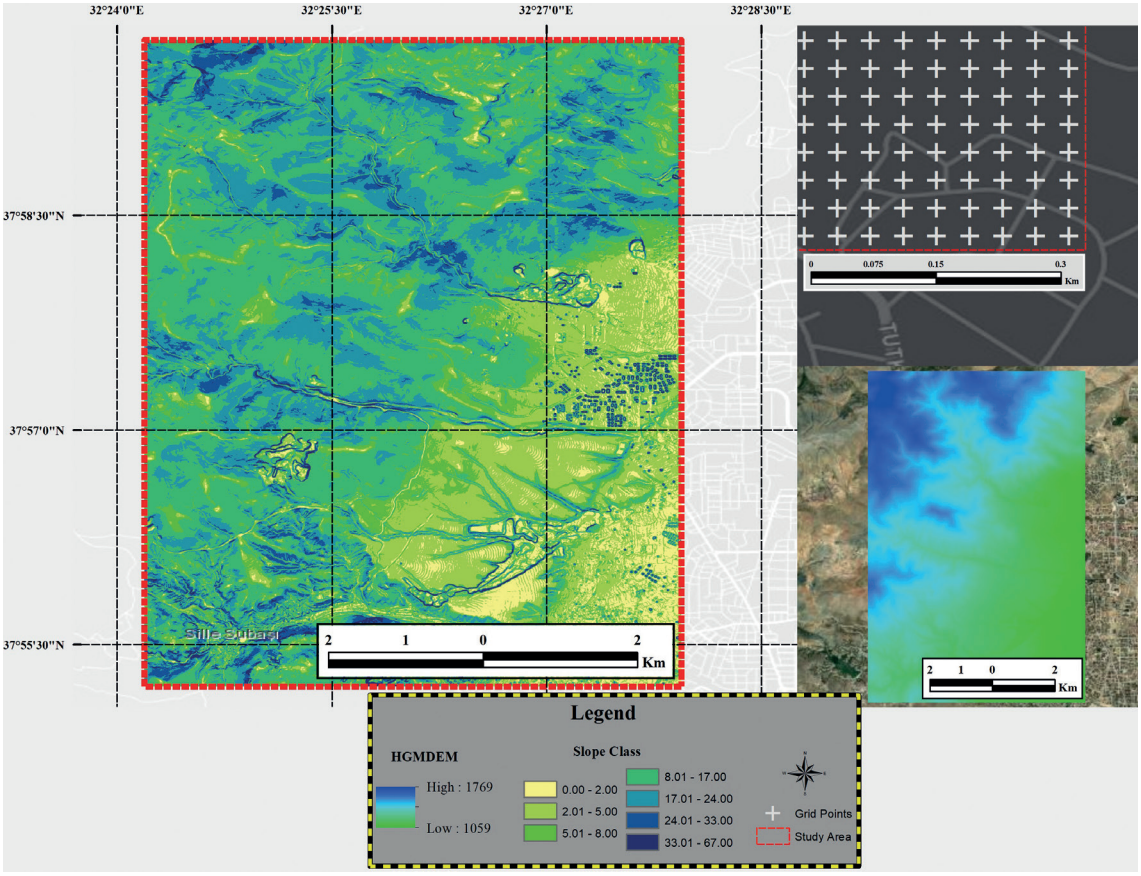

Fig. 1 - Study area: a) slope classes, b) generated grid points, and c) a DEM (HGMDEM).

the Earth's topography (including man-made structures and vegetation), which, in turn, was created by the radar interferometry method from Tandem-X and TerraSAR-X satellites. The creations are based on areas (latitude and longitude origins) covering 1°×1°. They have a ground sampling range of 1/3 arcsecond (approximately 12 m), horizontal position accuracy of ±5-10 m, and absolute height accuracy of ±4 m (Collins *et al*., 2015; Becek *et al*., 2016; Bayburt *et al*., 2017; Farooq *et al*., 2019).

2.4. Optical data

PlanetScope optical satellite data, used as a visual basemap in the study, is four-band (RGB + NIR) multispectral data that is provided free of charge for academic purposes, and is used to obtain multiple RGB data (Baloloy *et al*., 2018; Roy *et al*., 2021). By using RGB data, visual information, such as CORINE classes and information about the structure and terrain, was checked during the study, and care was taken to avoid gross mistakes (Fig. 2).

2.5. CORINE data

CORINE, used to determine land classes and perform accurate analyses of elevation models according to classes in this study, is land cover/use data produced by computer-aided visual

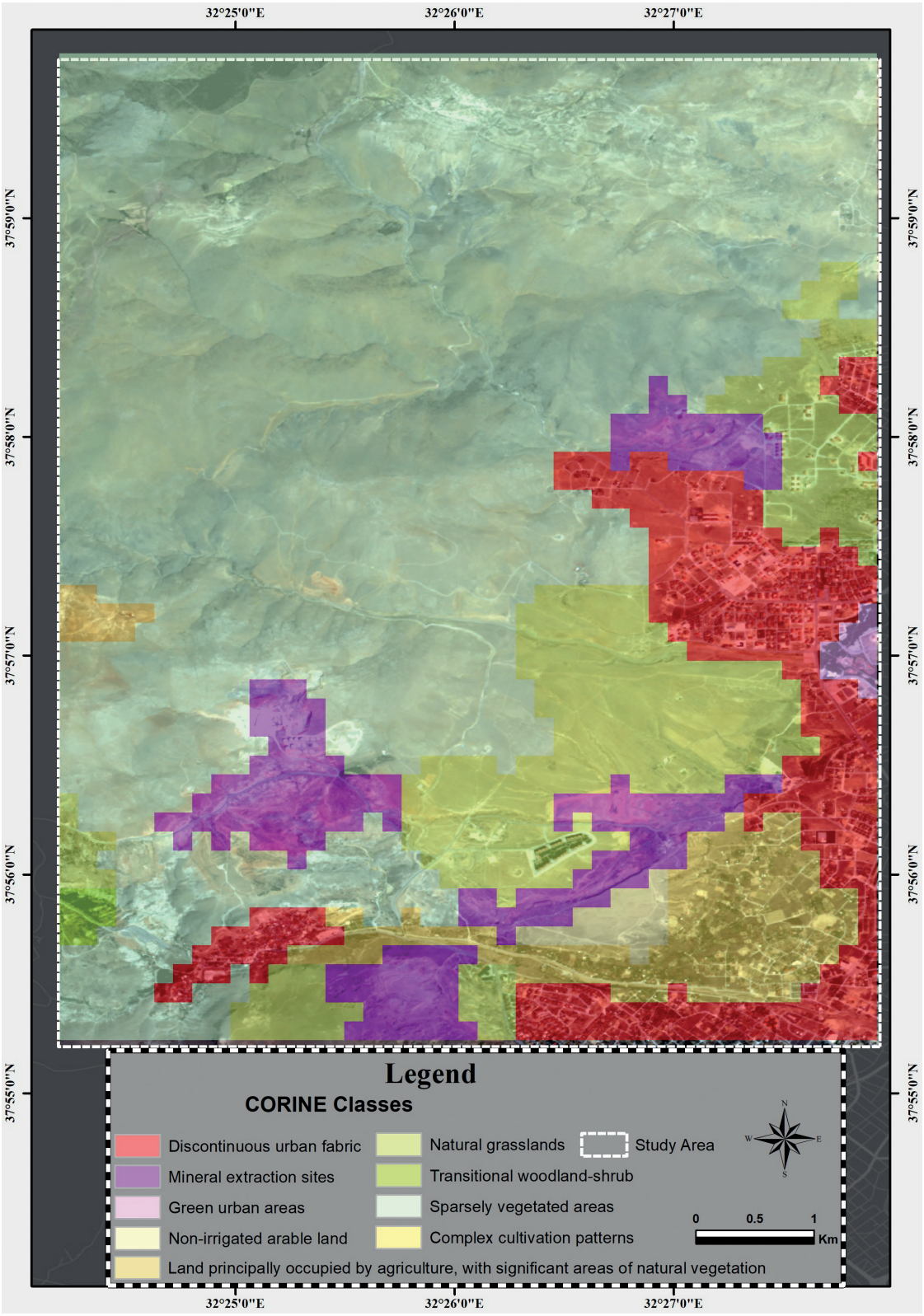

Fig. 2 - CORINE classes integrated with RGB PlanetScope optical image within the study area.

interpretation methods over satellite images according to the Land Cover/Use Classification determined by the European Environment Agency (Balzter *et al*., 2015; Kosztra *et al*., 2017; Tayebi *et al*., 2017). Corrected CLC2018 data Version 20 (Release date 24 February 2020), covering the study area, was used. Nine different classes from the CORINE classes have been selected for this study area (Fig. 2). These classes and their abbreviations are the following:

- complex cultivation patterns (CCP),
- discontinuous urban fabric (DUF),
- green urban areas (GUA),
- land principally occupied by agriculture, with significant areas of natural vegetation (LPO),
- mineral extraction sites (MES),
- natural grasslands (NGR),
- non-irrigated arable land (NAL),
- sparsely vegetated areas (SVA),
- transitional woodland-shrub (TWS).

The 43,750 grid points produced for the study area were distributed into the selected CORINE classes, and more precisely: 2,206 to CCP, 4,543 to DUF, 192 to GUA, 204 to LPO, 3,183 to MES, 5,624 to NGR, 345 to NAL, 27,314 to SVA, and 148 to TWS.

2.6. Statistical accuracy analysis

For the statistical accuracy analysis, *min* and *max* columns were created in the tables to determine the smallest and largest values of the sample set, respectively. These are the statistical minimum, also known as the low outlier limit, and the statistical maximum, also known as the high outlier limit. On the contrary, the mean value (μ) used in the analysis is expressed as the sum of all the components of the sample set divided by the number of samples (arithmetic mean):

$$\mu = \frac{1}{n}\sum_{i=1}^{n} \chi_{i.} \tag{1}$$

where *n* represents the total number of samples.

The sample value between the minimum and maximum values in the sample data series, dividing the string in half, is known as the median (med). It was utilised in this study to calculate the data set kurtosis value. The term *SD* is widely used in statistics to refer to the variance or distribution of numbers. Low standard deviation readings typically range slightly outside the sample group mean (estimated value). Conversely, a high standard indicates that the values are dispersed over a wider range. *SD* is represented by the Greek letter σ. In Eq. 2, the mathematical model of *SD* is presented:

$$\sigma = \sqrt{\frac{1}{n}[(\chi_1 - \mu)^2 + (\chi_2 - \mu)^2 + \cdots + (\chi_n - \mu)^2]}. \tag{2}$$

The mean-square error (*MSE*) of an estimator (i.e. a method for estimating an unobserved variable), or the average-squared difference between the estimated values and the actual values, is calculated as:

$$MSE = \frac{1}{n}\sum_{i=1}^{n}(\Upsilon_i - \hat{\Upsilon}_i)^2 \quad (3)$$

where Y is the vector of the observed values and $\hat{Y}$ is the vector of the predicted ones.

To determine the differences between the values predicted by a model, or the calculation of sample values, and the calculated values, one of the most widely used statistical analysis models is the *RMSE*. The *RMSE* of estimator $\hat{\Theta}$, with respect to estimated parameter Θ, is defined as the square root of the *MSE*:

$$RMSE(\hat{\Theta}) = \sqrt{MSE(\hat{\Theta})}. \quad (4)$$

The empirical rule, also referred to as the three-sigma rule (68-95-99.7), is a potential statistical rule used to determine the number of total values that fall within an interval calculation in a normal distribution, with 68%, 95%, and 99.7% of the values falling within one, two, and three *SD*, respectively.

2.7. DEM created from TerraSAR-X data

Two double ascending and two double descending TerraSAR-X satellite data sets were used to create TRXASC and TRXDSC DEMs (Table 1), as part of the European Space Agency (ESA) project (ID: 59832, entitled Filling Gaps in DEMs Produced from SAR Data with Different Orbital Properties and Resolution Using AI Algorithms). Data processing was carried out by the Sentinel Application Platform (SNAP), a free-of-charge software produced by ESA. A single datum was created from an image pair by coregistering the image pairs imported in the SNAP software. At this stage, the master and slave data, obtained as a result of the 'optimal reference' determined by the software, were approved, and a single "Coregistered Data" was produced from the two data. Then, the "Interferogram Creation" step was started using the coregistered data. The resulting output data, then, included coherence, phase, and intensity bands. The process was continued with the Goldstein Phase Filtering step, used to reduce the noise of the interferograms. The relatively noise-reduced data obtained was further processed with the Multilooking stage. Being a square pixel, each pixel of the output data produced by the SNAP software, as a result of this stage, presents a spatial resolution of approximately 2 m. Unwrapping followed, and the unwrapped phase interferogram band was obtained in the output data. In the "Phase to Elevation" step, the DEM was created by using the SRTM-1arcsecond data and resampling was performed with the Bilinear Interpolation technique. However, in order to use this DEM, it is necessary to convert it

Table 1 - Data specifications used for DEM creation.

Data type	Acquisition date	Orbit type	Data resolution (range × azimuth)
TSX-1.SAR.L1B	07 Apr 2020	Descending	1.2 m × 6.6 m
TSX-1.SAR.L1B	03 May 2020	Descending	1.2 m × 6.6 m
TSX-1.SAR.L1B	10 May 2020	Ascending	1.2 m × 6.6 m
TSX-1.SAR.L1B	21 May 2020	Ascending	1.2 m × 6.6 m

to the correct reference frame and coordinate system. Georeferenced output DEM was obtained by performing this with the "Terrain Correction" step (Fig. 3) (Fritz *et al*., 2008; Sefercik *et al*., 2014; Dong *et al*., 2021; Karabörk *et al*., 2021).

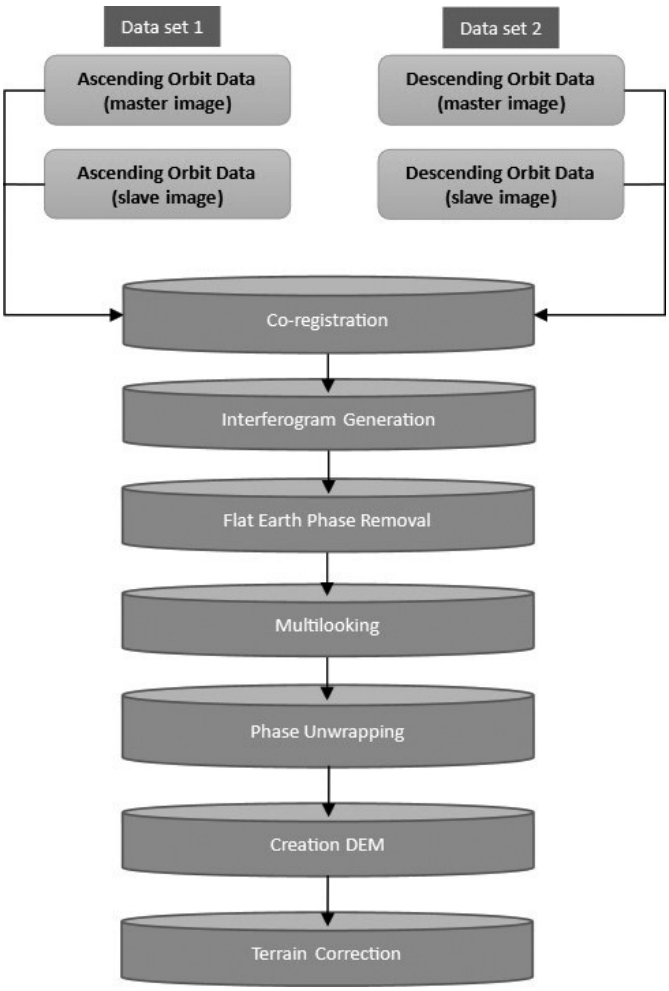

Fig. 3 - Workflow for the DEM creation used in the study for TRXASC and TRXDSC DEMs.

3. Results and discussions

In order to define the study workflow, elevation values for the grid points of the ready-to-use TWDEM and HGMDEM were calculated in tables, as well as the TRXDSC and TRXASC DEMs created using TerraSAR-X data acquired from the manufacturer. The study grid points were investigated from two angles on the basis of the CORINE and slope classes. The workflow chart displays every action taken during the investigation (Fig. 4).

The statistical results obtained from the differences of the TWDEM-HGMDEM, TRXDSC-HGMDEM, and TRXASC-HGMDEM for elevation values from all grid points (Tables 2 and 3) show that the DEM produced from the ascending orbit data provides better results than the DEM from the descending orbit data. The gross error points, determined according to the standard distribution, showed an increase in vertical position accuracy between 0.42 m and 0.95 m. The

differences between TWDEM and HGMDEM, produced the most accurate results throughout the entire study. When all slope classes are examined (Table 4), the 2-5° inclined class points reveal the highest accuracy results. Considering the points in the 95% confidence interval in accordance with the standard distribution of the grid points, the points belonging to the 2-5° inclined class offer the highest accuracy results (Table 5). When all grid points are examined with the CORINE classes, the TWDEM-HGMDEM difference reveals the highest accuracy results for the LPO class. For other differences, the GUA class provides the highest accuracy (Table 6). In Table 7, among the grid points examined in the 95% confidence interval, the CCP class showed the best results in TWDEM-HGMDEM differences. In contrast, the GUA class again showed the highest accuracy in other differences.

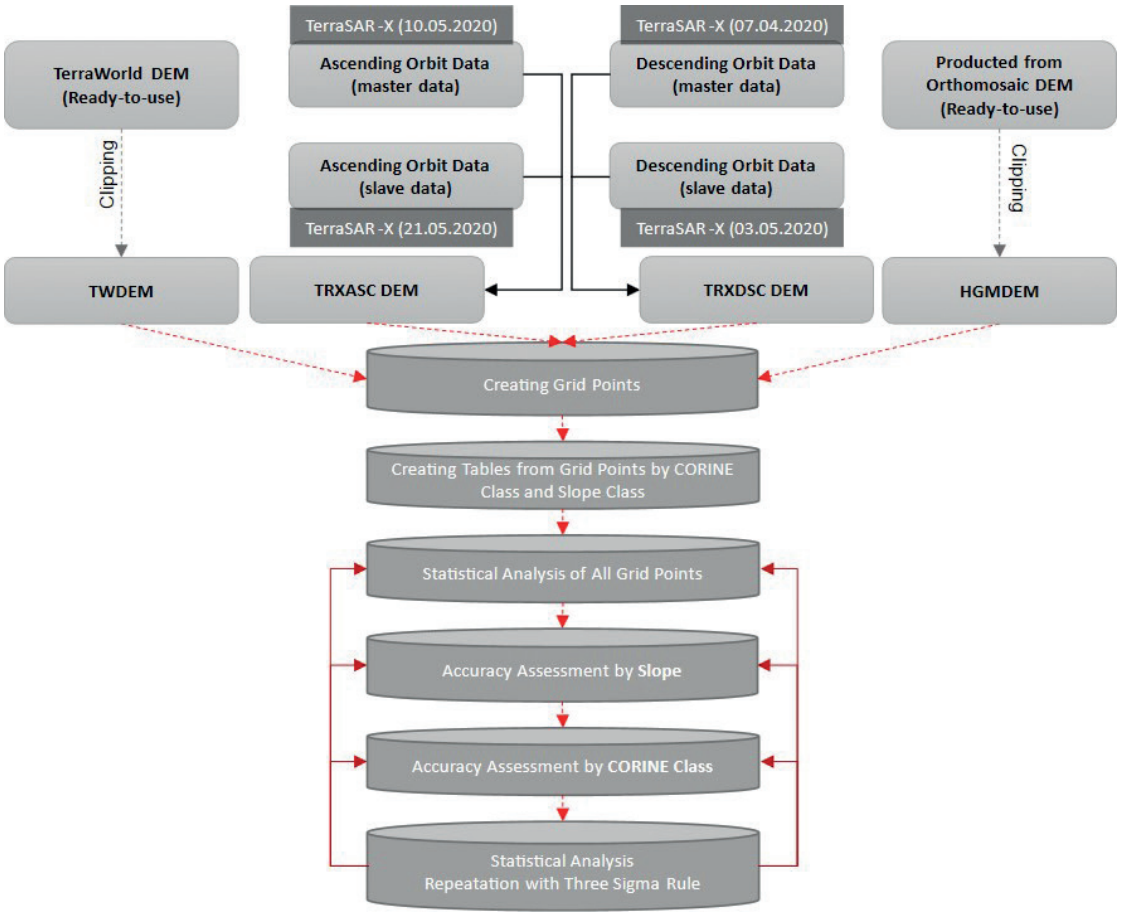

Fig. 4 - Workflow chart of the study.

According to the general statistical analysis results of 43,750 grid points representing the area, the differences with the highest accuracy in the *RMSE* and *SD* values are the differences between TWDEM and HGMDEM. According to the statistical analysis performed for two different image pairs with the same spatial resolution taken from descending and ascending orbits (Table 2), TRXASCDEM, the *SD*, and *RMSE* values indicate elevational differences with higher accuracy than TRXDSCDEM.

Table 2 - Statistical analysis of all grid points (units are expressed in m).

Differences	*Min*	*Max*	*Mean*	*Med*	*SD*	*RMSE*
TWDEM-HGMDEM	-18.04	21.26	-0.41	-0.41	1.41	1.47
TRXDSC-HGMDEM	-28.35	39.98	2.64	2.35	4.57	5.28
TRXASC-HGMDEM	-18.27	41.25	2.66	2.42	3.40	4.31

As a result, all these data were obtained in an office environment with the help of computers and, while they represent the land, they were not based on ground studies. Therefore, interpolation methods based on mathematical functions were used. Random elevation errors, due to interpolation techniques used in the production phase, occur as a result of the errors of data producers, or as a result of gross errors that may occur spontaneously from the terrain. Since it is impossible to individually detect random errors, accuracy analyses should be developed using statistical tools. Hence, considering the standard distribution of 43,750 grid points covering the entire test site, the number of points within the 95% confidence interval was determined (the number of points within the 95% confidence interval was 41,562 grid points). The statistical analysis results of the remaining 41,562 grid points, after the elimination of a total of 2,188 points outside the 95% confidence interval, according to the standard distribution charts, are presented in Table 3.

Table 3 - Statistical analysis of grid points at the 95% confidence interval (units are expressed in m).

Differences	*Min*	*Max*	*Mean*	*Med*	*SD*	*RMSE*
TWDEM-HGMDEM	-2.99	2.13	-0.42	-0.41	0.97	1.05
TRXDSC-HGMDEM	-6.36	12.69	2.46	2.32	3.56	4.33
TRXASC-HGMDEM	-3.68	9.45	2.49	2.40	2.48	3.52

An amount of 2,491 grid points was found to have slope angles between 0° and 2°. Of the total 43,750 grid points, 5.7% are made up of those 2,491 points. Likewise, the total number of grid points between slope angles of 2° and 5° is calculated as 7,232, representing 16.5% of the region on the grid. According to the analysis, there are 4,568 grid points overall with a slope angle between 5° and 8°. A total of 43,750 grid points represents the 4,368 points that make up the 5° to 8° slope region, which has a percentage of 10.4%. Also, 17,679 grid points were found to have a slope angle between 8° and 17°. An amount equal to 40% of the total is represented by the area having a slope between 8° and 17°, as indicated by the 17,679 points. In addition, 9,132 grid points totalled the slope angles of 17° to 24°. The area of 9,132 points represented has a 20% share of all grid points. The total number of grid points with a slope angle between 24° and 33° is calculated to be 2,130. The percentage of all grid points, in relation to the area covered by 2,130 points, is 4.9%. Between slope angles of 33° and 62°, there were 518 grid points. Last but not least, a slope of 33° to 62°, represented by 518 grid points out of 43,750, has a percentage of 1.2%. Statistical analysis results of seven different slope classes are shown in Table 4.

An amount of 2,366 grid points, with slope angles between 0° and 2°, were present within the 95% confidence range. After the elimination of 125 points outside the 5% confidence interval, in

Table 4 - Statistical analysis of all grid points according to slope classes (units are expressed in m).

Differences	*Min*	*Max*	*Mean*	*Med*	*SD*	*RMSE*	Slope Class
TWDEM-HGMDEM (1)	-9.65	19.98	-0.36	-0.44	1.16	1.21	0-2°
TRXDSC-HGMDEM (2)	-12.83	38.49	2.89	2.36	3.99	4.92	
TRXASC-HGMDEM (3)	-9.15	40.12	2.94	2.4	3.86	4.85	
TWDEM-HGMDEM (1)	-5.52	17.48	-0.39	-0.44	0.9	0.98	2-5°
TRXDSC-HGMDEM (2)	-12.1	37.76	2.36	2.21	3.3	4.06	
TRXASC-HGMDEM (3)	-7.73	38.77	2.51	2.33	2.83	3.78	
TWDEM-HGMDEM (1)	-15.72	21.26	-0.39	-0.39	1.03	1.1	5-8°
TRXDSC-HGMDEM (2)	-16.98	27.79	2.41	2.27	4.31	4.94	
TRXASC-HGMDEM (3)	-12.81	28.47	2.59	2.35	3.27	4.17	
TWDEM-HGMDEM (1)	-16.41	19.7	-0.39	-0.38	1.17	1.23	8-17°
TRXDSC-HGMDEM (2)	-20.52	39.98	2.19	2.09	4.58	5.04	
TRXASC-HGMDEM (3)	-14.16	40.72	2.49	2.33	3.19	4.04	
TWDEM-HGMDEM (1)	-12.4	10.49	-0.46	-0.42	1.6	1.67	17-24°
TRXDSC-HGMDEM (2)	-25.06	30.22	3.28	3	4.87	5.87	
TRXASC-HGMDEM (3)	-11.73	32.83	2.86	2.72	3.39	4.43	
TWDEM-HGMDEM (1)	-10.25	16.41	-0.48	-0.51	2.48	2.52	24-33°
TRXDSC-HGMDEM (2)	-28.35	34.75	4.33	4.07	6.28	7.63	
TRXASC-HGMDEM (3)	-18.27	37.73	3.4	3.24	4.64	5.75	
TWDEM-HGMDEM (1)	-18.04	18.78	-0.95	-1.29	4.79	4.87	33-62°
TRXDSC-HGMDEM (2)	-18.84	39.1	3.11	2.52	8.34	8.9	
TRXASC-HGMDEM (3)	-13.22	41.25	3.15	2.44	7.45	8.08	

accordance with the standard distribution charts, the statistical analysis findings of the region with a 0-2° slope, represented by the remaining 2,366 points, are shown in Table 4. Likewise, 6,870 grid points with slope angles between 2° and 5° fall within the 95% confidence range. The statistical analysis outcomes of the region with a slope of 2-5°, represented by the remaining 6,870 points, are shown in Table 4 after eliminating 362 points outside the 5% confidence interval. The number of points within the 95% confidence interval of all grid points with a slope angle of 5° to 8° was calculated as 4,340. The statistical analysis results of the region with a slope of 5° to 8°, represented by the remaining 4,340 points, after the elimination of a total of 228 points outside the 5% confidence interval according to the standard distribution charts, are presented in Table 4. In addition to these, the total number of grid points with slope angles ranging from 8° to 17°, that match within the 95% confidence range, is 16,795. The statistical analysis findings of the area with a slope of 8-17°, represented by the remaining 16,795 points, are shown in Table 4 after the elimination of a total of 884 points outside the 5% confidence interval in conformity with the standard distribution. There are 8,676 grid points with a slope angle between 17° and 24° that fall within the 95% confidence range. The statistical analysis results of the region with a slope of 17-24°, represented by the remaining 8,676 points after the elimination of a total of 456 points outside the 5% confidence interval according to the standard distribution charts, are presented in Table 4. The total number of grid points with a slope angle between 24° and 33°, that fall within the 95% confidence range, is 2,025. Following the elimination of 105 points outside the 5% confidence range based on the standard distribution intervals, the statistical analysis findings of the region with a slope of 24-33°, represented by

the remaining 2,025 points, are shown in Table 4. There are 493 grid points with a slope angle between 33° and 62° that fall within the 95% confidence range. Lastly, the statistical analysis results of the region with a 33-62° slope, represented by the remaining 493 points after the elimination of a total of 25 points outside the 5% confidence interval according to the standard distribution intervals, are presented in Table 5.

Table 5 - Statistical analysis of grid points with the 95% confidence interval according to slope classes (units are expressed in m).

Differences	*Min*	*Max*	*Mean*	*Med*	*SD*	*RMSE*	Slope Class
TWDEM-HGMDEM (1)	-1.46	1.37	-0.41	-0.43	0.45	0.61	0-2°
TRXDSC-HGMDEM (2)	-3.81	13.21	2.47	2.34	2.14	3.26	
TRXASC-HGMDEM (3)	-2.19	11.15	2.47	2.37	1.87	3.1	
TWDEM-HGMDEM (1)	-1.49	0.86	-0.43	-0.44	0.45	0.62	2-5°
TRXDSC-HGMDEM (2)	-3.92	9.98	2.15	2.2	2.02	2.95	
TRXASC-HGMDEM (3)	-2.07	7.97	2.32	2.32	1.73	2.9	
TWDEM-HGMDEM (1)	-1.92	1.25	-0.38	-0.38	0.63	0.74	5-8°
TRXDSC-HGMDEM (2)	-6.01	11.95	2.21	2.24	3.31	3.98	
TRXASC-HGMDEM (3)	-3.26	9.1	2.41	2.33	2.38	3.39	
TWDEM-HGMDEM (1)	-2.47	1.69	-0.39	-0.38	0.92	1	8-17°
TRXDSC-HGMDEM (2)	-6.49	11.77	2.11	2.05	3.63	4.2	
TRXASC-HGMDEM (3)	-3.51	8.96	2.39	2.31	2.48	3.44	
TWDEM-HGMDEM (1)	-3.43	2.51	-0.44	-0.42	1.35	1.42	17-24°
TRXDSC-HGMDEM (2)	-6.42	13.21	3.19	2.97	4.06	5.16	
TRXASC-HGMDEM (3)	-3.64	9.59	2.79	2.7	2.72	3.89	
TWDEM-HGMDEM (1)	-4.99	4.11	-0.45	-0.49	1.98	2.03	24-33°
TRXDSC-HGMDEM (2)	-9	15.97	4.06	3.98	5.39	6.74	
TRXASC-HGMDEM (3)	-6.68	11.98	3.22	3.17	3.72	4.92	
TWDEM-HGMDEM (1)	-8.74	11.82	-0.79	-1.26	3.85	3.93	33-62°
TRXDSC-HGMDEM (2)	-9.88	22.47	3.26	2.62	7.24	7.93	
TRXASC-HGMDEM (3)	-9.17	20.23	2.8	2.39	6.09	6.69	

The statistical accuracy analysis of 43,750 grid points, grouped in nine CORINE classes, are presented in Table 6, which lists the differences of TWDEM-HGMDEM, TRXDSC-HGMDEM, and TRXASC-HGMDEM, respectively.

The number of points within the 95% confidence interval of 43,750 grid points, covering the entire study area, was determined as 41,562. Table 7 shows the statistical analysis results of the remaining 41,562 points, according to the CORINE classes, after eliminating 2,188 points outside the 5% confidence interval according to the standard distribution charts.

In the literature, no studies on the comparison of DEMs using CORINE classes could be found. For this reason, essential findings regarding DEM differences related to CORINE classes have been revealed. It can be said that there are significant differences in data resolution between DEMs produced with CORINE data. However, CORINE classes contributed significantly as DEMs were evaluated as a different class compared to the studies with classical slope classes, and improved the aim of the study. If we consider the other studies in the literature with slope classes, the high

Table 6 - Statistical accuracy analysis for the differences of all grid points belonging to the CORINE classes.

CORINE CLASS	*Min*	*Max*	*Mean*	*Med*	*SD*	*RMSE*	
CCP	-16.41	5.73	-0.41	-0.35	1.02	1.10	
DUF	-17.74	9.79	-0.72	-0.53	1.64	1.80	
GUA	-9.11	10.70	-0.91	-0.77	1.62	1.86	
LPO	-2.59	2.49	-0.32	-0.28	0.82	0.88	
MES	-18.04	21.26	-0.41	-0.54	2.19	2.23	TerraWorld-HGM
NGR	-9.19	13.40	-0.50	-0.49	0.95	1.07	
NAL	-4.02	1.61	-0.58	-0.58	0.61	0.84	
SVA	-15.23	19.70	-0.34	-0.34	1.35	1.40	
TWS	-5.11	5.14	-0.30	-0.41	1.40	1.43	
CCP	-13.60	13.91	2.58	2.50	2.60	3.67	
DUF	-15.47	23.52	2.10	2.30	2.89	3.57	
GUA	-7.11	6.95	1.29	1.36	2.03	2.38	
LPO	-8.32	11.71	3.84	3.91	2.87	4.79	
MES	-16.36	39.98	4.67	3.40	6.83	8.27	TRXDSC-HGM
NGR	-28.35	29.18	2.38	2.30	3.15	3.95	
NAL	-6.27	8.51	1.08	1.63	2.62	2.83	
SVA	-25.06	30.10	2.58	2.31	4.80	5.45	
TWS	-13.15	20.37	2.61	2.58	5.51	6.08	
CCP	-14.16	11.28	2.25	2.33	2.05	3.01	
DUF	-13.22	24.96	2.04	2.24	2.66	3.35	
GUA	-9.11	10.70	-0.92	-0.77	1.70	2.39	
LPO	-2.99	9.03	3.40	3.22	2.34	4.12	
MES	-9.43	41.25	4.64	3.07	6.33	7.85	TRXASC-HGM
NGR	-18.27	29.05	2.45	2.38	2.57	3.54	
NAL	-6.59	8.07	1.55	2.08	2.41	2.86	
SVA	-15.03	31.93	2.63	2.45	3.19	4.13	
TWS	-5.99	13.74	2.54	2.52	3.48	4.30	

vertical accuracy seen between 0° and 8°, which is generally considered very slightly sloped, was also increased, as expected in this study. In the literature, studies with slope classes are usually divided into low slope areas (0-8°), medium slope areas (8-25°), and high slope areas (25° and above) (Birhanu *et al*., 2019; Fuentes *et al*., 2019; Kramm and Hoffmeister, 2019; Uuemaa *et al*., 2020). This study tried to find a suitable response for almost all land slope classes with divided slope classes. The slope classes selected, according to the structure of the study area, were created by paying attention to the homogeneous selection of the points (Birhanu *et al*., 2019; Graham *et al*., 2019; Alvioli *et al*., 2020; Gdulová *et al*., 2020; Gümüs *et al*., 2021). In this way, the behaviour of the DEMs, obtained from different sources in the sub-slope groups, has been observed.

According to the accuracy analysis of the DEMs obtained from the high-resolution SAR data, the results of the research made according to the slope classes, and the DEMs produced from the data obtained from both ascending and descending orbits with TerraSAR data offer a higher spatial resolution. Vertical positional accuracy varies between 3-5 m and 8-10 m (depending on

Table 7 - Statistical accuracy analysis of grid points at a 95% confidence interval of the CORINE classes.

CORINE CLASS	*Min*	*Max*	*Mean*	*Med*	*SD*	*RMSE*	
CCP	-2.20	1.37	-0.37	-0.35	0.65	0.75	
DUF	-4.63	1.81	-0.61	-0.54	0.89	1.07	
GUA	-3.50	1.35	-0.83	-0.77	0.85	1.18	
LPO	-1.89	1.36	-0.33	-0.28	0.70	0.77	
MES	-3.68	5.29	-0.46	-0.49	1.33	1.39	TerraWorld-HGM
NGR	-2.35	1.32	-0.50	-0.50	0.60	0.77	
NAL	-1.87	0.59	-0.57	-0.58	0.48	0.74	
SVA	-2.88	2.19	-0.34	-0.33	1.05	1.11	
TWS	-2.95	2.88	-0.29	-0.41	1.12	1.16	
CCP	-3.97	7.81	2.47	2.46	1.96	3.15	
DUF	-5.98	7.37	2.05	2.24	2.15	2.96	
GUA	-3.60	4.76	1.31	1.47	1.62	2.08	
LPO	-2.74	8.85	3.83	3.88	2.34	4.48	
MES	-6.73	20.30	4.44	3.56	5.70	7.10	TRXDSC-HGM
NGR	-4.30	8.59	2.28	2.23	2.22	3.17	
NAL	-4.46	6.39	1.03	1.62	2.25	2.48	
SVA	-6.61	12.90	2.41	2.25	3.93	4.63	
TWS	-9.94	16.78	2.47	2.57	4.47	5.09	
CCP	-3.19	5.69	2.21	2.29	1.65	2.76	
DUF	-5.24	6.48	2.02	2.15	2.05	2.86	
GUA	-3.06	4.23	1.27	1.33	1.60	2.04	
LPO	-0.92	7.74	3.35	3.21	2.10	3.95	
MES	-4.45	21.18	4.30	3.18	5.04	6.51	TRXASC-HGM
NGR	-2.55	7.06	2.35	2.32	1.85	2.99	
NAL	-4.02	5.65	1.53	2.05	2.09	2.58	
SVA	-3.56	9.15	2.52	2.41	2.56	3.61	
TWS	-4.78	9.63	2.47	2.52	3.02	3.8	

terrain type or terrain class) in recent SAR data and high-resolution DEM generation surveys (Erten *et al*., 2018; Malik and Kumar, 2018; Torun and Orhan, 2021; Torun, 2022). In this study, the vertical positional accuracy values of 3.5-4.0 m were reached robustly after eliminating gross errored points.

When analysing results with *RMSE*, it can be seen that areas with 0-2° slope deliver more unsatisfactory results than areas with 2-5° slope. Similar results are found when this evaluation is made within the 95% confidence interval. Here, it can be said that there is no significant metric difference between 0-2° and 2-5° in land classes. According to the slope classes, the main difference is seen in areas with slopes greater than 8°. In CORINE classes, instead, systematically similar things are not observed. Classes offer varying degrees of variation within themselves.

Although the CORINE class classification type adopted here has never been used in a DEM accuracy analysis in the literature, it has been determined to offer very understandable results. For example, according to CORINE, since the surfaces in the MES class have dynamic processes, cumulative DEM production errors are observed in the large mine sites, more precisely, in MES

class areas located to the west and south of the study area (Fig. 2). As a result, DEM products realised with remote sensing have gross *RMSE* values in these classes. Conversely, the NAL class is a field type where the *RMSE* can be minimal in terms of DEM realised techniques. Good results are expected in these areas, which are generally barren areas, with no man-made objects. The lack of this information in the studies in the literature is a significant shortcoming. But it is also one of the most important original results of this study.

4. Conclusions

In this study, in which DEMs obtained from different sources were determined as the subject of vertical spatial accuracy assessment, DEMs, produced from ascending and descending orbit TerraSAR-X (TRXASC DEM and TRXDSC DEM) data pairs, and worldwide DEM (TWDEM), obtained from TanDEM-X data, were subjected to accuracy analysis. The basemap DEM, used to determine the accuracies, is the aerial photogrammetry-sourced DEM obtained by the national manufacturer, i.e. the general directorate of maps (HGMDEM). According to the research results obtained from the 43,750 grid points produced in the common layers, it has been revealed that TWDEM provides high accuracy results**.** TWDEM delivers elevational differences below 1-metre accuracy when total gross error points are eliminated from the 95% confidence interval, and are discarded according to the standard distribution.

Accuracy analysis has been developed with two different classifications: slope classes and CORINE classes. The results show that TWDEM provides the most accurate results for all grid points and points with 95% confidence intervals in all slope groups.

Acknowledgments. The data used in this research were provided free of charge within the scope of "Filling Gaps in DEMs Produced from SAR Data with Different Orbital Properties and Resolutions Using AI Algorithms", European Space Agency (ESA) CAT1 - Project 59832. CORINE Turkey data has been updated by the Ministry of Agriculture and Forestry for the European Environment Agency (EEA). I would sincerely like to thank ESA and EEA for providing the data. For all their contributions, I am also grateful to PlanetScope satellite systems, which provide free-of-charge optical satellite data for academic use. The data presented in this study are available on request to the author. Data are not publicly available.

REFERENCES

Akturk E. and Altunel A.O.; 2019: *Accuracy assessment of a low-cost UAV derived digital elevation model (DEM) in a highly broken and vegetated terrain*. Meas., 136, 382-386., in Turkish.

Altunel A.O.; 2019: *Evaluation of TanDEM-X 90 m digital elevation model*. Int. J. Remote Sens., 40, 2841-2854.

Alvioli M., Guzzetti F. and Marchesini I.; 2020: *Parameter-free delineation of slope units and terrain subdivision of Italy*. Geomorphol., 358, 107124, 20 pp., doi: 10.1016/j.geomorph.2020.107124.

Amami M., Elmehdwi A.I., Borgaa A.I., Buker A.F. and Alareibi A.S.; 2022: *Investigations into utilizing low-cost amateur drones for creating ortho-mosaic and digital elevation model.* Int. Res. J. Mod. Eng. Tech. Sci., 4, 2107-2118.

Atkinson P.M., Stein A. and Jeganathan C.; 2022: *Spatial sampling, data models, spatial scale and ontologies: interpreting spatial statistics and machine learning applied to satellite optical remote sensing.* Spatial Stat., 50, 100646, 21 pp., doi: 10.1016/j.spasta.2022.100646.

Balasubramanian A.; 2017: *Digital elevation model (DEM) in GIS*. Centre for Advanced Studies in Earth Science, University of Mysore, Mysore, India, 33 pp., doi: 10.13140/RG.2.2.23976.47369.

Baloloy A.B., Blanco A.C., Candido C.G., Argamosa R.J.L., Dumalag J.B.L.C., Dimapilis L.L.C. and Paringit E.C.; 2018: *Estimation of mangrove forest aboveground biomass using multispectral bands, vegetation indices and biophysical variables derived from optical satellite imageries: Rapideye, Planetscope and Sentinel-2.* In: Proc. SPRS TC III Mid-term Symposium Developments, Technologies and Applications in Remote Sensing, Beijing, China, ISPRS Ann. Photogramm., Remote Sens. Spatial Inf. Sci., 4, 8 pp., doi: 10.5194/isprs-annals-IV-3-29-2018.

Balzter H., Cole B., Thiel C. and Schmullius C.; 2015: *Mapping CORINE land cover from Sentinel-1A SAR and SRTM digital elevation model data using Random Forests.* Remote Sens., 7, 14876-14898, doi: 10.3390/rs71114876.

Basu B.; 2021: *Development of soil and land cover databases for use in the soil water assessment tool from Irish National soil maps and CORINE land cover maps for Ireland*. Earth Syst. Sci. Data Discuss., 19 pp., doi: 10.5194/essd-2021-169.

Bayburt S., Kurtak A., Büyüksalih G. and Jacobsen K.; 2017: *Geometric accuracy analysis of WorldDEM in relation to AW3D30, SRTM and ASTER GDEM2.* Int. Arch. Photogramm., Remote Sens. Spatial Inf. Sci., XLII-1/W1, 211-217, doi: 10.5194/isprs-archives-XLII-1-W1-211-2017.

Becek K., Koppe W. and Kutoğlu Ş.H.; 2016: *Evaluation of vertical accuracy of the WorldDEM™ using the Runway method.* Remote Sens., 8, 934, 12 pp., doi: 10.3390/rs8110934.

Birhanu L., Hailu B.T., Bekele T. and Demissew S.; 2019: *Land use/land cover change along elevation and slope gradient in highlands of Ethiopia.* Remote Sens. Appl.: Soc. Environ., 16, 100260, 9 pp., doi: 10.1016/j.rsase.2019.100260.

Chen C., Liu F., Li Y., Yan C. and Liu G.; 2016: *A robust interpolation method for constructing digital elevation models from remote sensing data*. Geomorphol., 268, 275-287.

Chu T. and Lindenschmidt K.-E.; 2017: *Comparison and validation of digital elevation models derived from InSAR for a flat inland delta in the high latitudes of northern Canada.* Can. J. Remote Sens., 43, 109-123.

Chymyrov A.; 2021: *Comparison of different DEMs for hydrological studies in the mountainous areas.* Egypt. J. Remote Sens. Space Sci., 24, 587-594.

Collins J., Riegler D.G., Schrader H. and Tinz M.; 2015: A*pplying terrain and hydrological editing to tandem-x data to create a consumer-ready worlddem product*. In: Proc. 36th International Symposium on Remote Sensing of Environment, Berlin, Germany, Int. Arch. Photogramm., Remote Sens. Spatial Inf. Sci., XL-7/W3, 1149-1154, doi: 10.5194/isprsarchives-XL-7-W3-1149-2015.

Cosandier D.D.; 1999: *Generating a digital elevation model and orthomosaic from pushbroom imagery*. Ph.D. Thesis in Geomatics Engineering., University of Calgary, Canada, 275 pp.

Courty L.G., Soriano-Monzalvo J.C. and Pedrozo-Acuña A.; 2019: *Evaluation of open-access global digital elevation models (AW3D30, SRTM, and ASTER) for flood modelling purposes.* J. Flood Risk Manage., 12, e12550, 26 pp., doi: 10.31223/osf.io/vqgx4.

Das S., Patel P.P. and Sengupta S.; 2016: *Evaluation of different digital elevation models for analyzing drainage morphometric parameters in a mountainous terrain: a case study of the Supin–Upper Tons Basin, Indian Himalayas*. SpringerPlus, 5, 1544, 38 pp., doi: 10.1186/s40064-016-3207-0.

Di Lascio F.M.L., Falchetta G. and Ferrari D.; 2022: *Change detection from high-resolution airborne laser scans using penalized composite likelihood screening*. Spatial Stat., 52, 100710, 18 pp., doi: 10.1016/j.spasta.2022.100710.

Dong Y., Zhang L., Jiang H., Balz T. and Liao M.; 2021: *Cascaded multi-baseline interferometry with bistatic TerraSAR-X/TanDEM-X observations for DEM generation.* ISPRS J. Photogramm. Remote Sens., 71, 224-237, doi: 10.1016/j.isprsjprs.2020.11.012.

Eckert S., Kellenberger T. and Itten K.; 200*5: Accuracy assessment of automatically derived digital elevation models from aster data in mountainous terrain.* Int. J. Remote Sens., 26, 1943-1957.

El-Quilish M., El-Ashquer M., Dawod G. and Fiky G.E.; 2023: *Development of an inundation model for the northern coastal zone of the Nile Delta region, Egypt using high-resolution DEM.* Arabian J. Sci. Eng., 48, 601-614.

Erten E., Çelik M.F. and Şahin Z.M.; 2018: *TanDEM-X Digital Elevation Model Generation*. Harita Dergisi, 84, 47-54, in Turkish.

Farooq M., Shafique M. and Khattak M.S.; 2019: *Flood hazard assessment and mapping of River Swat using HEC-RAS 2D model and high-resolution 12-m TanDEM-X DEM (WorldDEM).* Nat. Hazards, 97, 477-492.

Fritz T., Breit H., Adam N., Eineder M. and Lachaise M.; 2008. *Interferometric SAR processing: from TerraSAR-X to TanDEM-X.* In: Proc. 7th European Conference on Synthetic Aperture Radar, Friedrichshafen, Germany, pp. 1-4.

Fuentes I., Padarian J., van Ogtrop F. and Vervoort R.W.; 2019: *Comparison of surface water volume estimation methodologies that couple surface reflectance data and digital terrain models.* Water, 11, 780, 19 pp., doi: 10.3390/w11040780.

Gdulová K., Marešová J. and Moudrý V.; 2020: *Accuracy assessment of the global TanDEM-X digital elevation model in a mountain environment.* Remote Sens. Environ., 241, 111724, 15 pp., doi: 10.1016/j.rse.2020.111724.

Gelfand A.E.; 2022: *Spatial modeling for the distribution of species in plant communities.* Spatial Stat., 50, 100582, 17 pp., doi: 10.1016/j.spasta.2021.100582.

Graham A., Coops N.C., Wilcox M. and Plowright A.; 2019: *Evaluation of ground surface models derived from unmanned aerial systems with digital aerial photogrammetry in a disturbed conifer forest.* Remote Sens., 11*,* 84, 19 pp., doi: 10.3390/rs11010084.

Gümüs M., Durduran S. and Gümüs K.; 2021: *Investigation of shoreline change rates using the digital shoreline analysis system in Lake Beyşehïr, Turkey.* Bull. Geoph. Ocean., 63, 119-142, doi: 10.4430.bgo00369.

Habib M., Alzubi Y., Malkawi A. and Awwad M.; 2020: *Impact of interpolation techniques on the accuracy of large-scale digital elevation model*. Open Geosci., 12, 190-202, doi: 10.1515/geo-2020-0012.

Hilton R.D., Featherstone W.E., Berry P.A.M., Johnson C.P.D. and Kirby J.F.; 2003: *Comparison of digital elevation models over Australia and external validation using ERS-1 satellite radar altimetry.* Aust. J. Earth Sci., 50, 157-168.

Huqqani I.A., Tay L.T. and Mohamad-Saleh J.; 2022: *Assessment of landslide susceptibility mapping using artificial bee colony algorithm based on different normalizations and dimension reduction techniques*. Arabian J. Sci. Eng., 47, 7243-7260.

Ibrahim S.A; 2023: *Improving land use/cover classification accuracy from random forest feature importance selection based on synergistic use of sentinel data and digital elevation model in agriculturally dominated landscape.* Agric., 13, 98, 22 pp., doi: 10.3390/agriculture13010098.

Karabörk H., Makineci H.B., Orhan O. and Karakus P.; 2021: *Accuracy assessment of DEMs derived from multiple SAR data using the InSAR technique*. Arabian J. Sci. Eng., 46, 5755-5765.

Konya O., Arıcan D., Uzar M., Soysal H.O. and Eken V.; 2018: *Production of digital elevation model by aerial photogrammetry and geodetic methods: the example of the Erzurum aksu village*. In: Proc. TMMOB Harita ve Kadastro Mühendisleri Odası, 16. Türkiye Harita Bilimsel ve Teknik Kurultayı, Ankara, Turkey, 6 pp., in Turkish.

Kosztra B., Büttner G., Hazeu G. and Arnold S.; 2017: *Updated CLC illustrated nomenclature guidelines*. European Topic Centre on Urban, land and soil systems, ETC/ULS, Environment Agency, Wien, Austria, Service Contract No 3436/R0-Copernicus/EEA.57441 Task 3, D3.1 - Part 1, 126 pp.

Kramm T. and Hoffmeister D.; 2019: *A relief dependent evaluation of digital elevation models on different scales for northern Chile*. ISPRS Int. J. Geo-Inf., 8, 430, 25 pp., doi: 10.3390/ijgi8100430.

Kumar A., Negi H.S., Kumar K., Shekhar C. and Kanda N.; 2019: *Quantifying mass balance of east-Karakoram glaciers using geodetic technique*. Polar Sci., 19, 24-39.

Lee K.S., Lee G.B. and Tyler E.; 1988: *Thematic mapper and digital elevation modeling of soil characteristics in hilly terrain*. Soil Sci. Soc. Am. J., 52, 1104-1107.

Li H., Zhao J., Yan B., Yue L. and Wang L.; 2022: *Global DEMs vary from one to another: an evaluation of newly released Copernicus, NASA and AW3D30 DEM on selected terrains of China using ICESat-2 altimetry data.* Int. J. Digital Earth, 15, 1149-1168.

Liu H., Jezek K.C. and Li B.; 1999: *Development of an Antarctic digital elevation model by integrating cartographic and remotely sensed data: a geographic information system based approach*. J. Geophys. Res.: Solid Earth, 104, 23199-23213.

Luo H., Li Z., Dong Z., Liu P., Wang C. and Song J.; 2020: *A new baseline linear combination algorithm for generating urban digital elevation models with multitemporal InSAR observations.* IEEE Trans. Geosci. Remote Sens., 58, 1120-1133.

Makineci H.B. and Karabörk H.; 2016: *Evaluation digital elevation model generated by synthetic aperture radar data.* Int. Arch. Photogramm., Remote Sens. Spatial Inf. Sci., 1, 57-62.

Malik K. and Kumar D.; 2018: *High resolution interferometric digital elevation model generation and validation*. In: Proc. ISPRS TC V Mid-term Symposium Geospatial Technology - Pixel to People, Dehradun, India, Int. Arch. Photogramm., Remote Sens. Spatial Inf. Sci., Vol. XLII-5, 2 pp.

Mason D.C., Dance S.L. and Cloke H.L.; 2021: *Floodwater detection in urban areas using Sentinel-1 and World-DEM data*. J. Appl. Remote Sens., 15, 032003, 22 pp., doi: 10.1117/1.JRS.15.032003.

Mukherjee S., Joshi P.K., Mukherjee S., Ghosh A., Garg R.D. and Mukhopadhyay A.; 2013: *Evaluation of vertical accuracy of open source Digital Elevation Model (DEM).* Int. J. Appl. Earth Obs. Geoinf., 21, 205-217.

Muthusamy M., Casado M.R., Butler D. and Leinster P.; 2021: *Understanding the effects of digital elevation model resolution in urban fluvial flood modelling*. J. Hydrol., 596, 126088, 15 pp., doi: 10.1016/j.jhydrol.2021.126088.

Nardò S., Ascione A., Mazzuoli S., Terranova C. and Vilardo G.; 2020: *PS-InSAR data analysis: pre-seismic ground deformation in the 2009 L'Aquila earthquake region.* Boll. Geof. Teor. Appl., 61, 41-56, doi: 10.4430/bgta0251.

Polidori L. and El Hage M.; 2020: *Digital elevation model quality assessment methods: a critical review.* Remote Sens., 12, 3522, 36 pp., doi: 10.3390/rs12213522.

Rabus B., Eineder M., Roth A. and Bamler R.; 2003: *The shuttle radar topography mission—a new class of digital elevation models acquired by spaceborne radar.* ISPRS J. Photogramm. Remote Sens., 57, 241-262.

Rocha J., Duarte A., Silva M., Fabres S., Vasques J., Revilla-Romero B. and Quintela A.; 2020: *The importance of high resolution digital elevation models for improved hydrological simulations of a Mediterranean forested catchment.* Remote Sens., 12, 3287, 17 pp., doi: 10.3390/rs12203287.

Roy D.P., Huang H., Houborg R. and Martins V.S.; 2021: *A global analysis of the temporal availability of PlanetScope high spatial resolution multi-spectral imagery.* Remote Sens. Environ., 264, 112586, 21 pp., doi: 10.1016/j.rse.2021.112586.

Salekin S., Burgess J.H., Morgenroth J., Mason E.G. and Meason D.F.; 2018: *A comparative study of three non-geostatistical methods for optimising digital elevation model interpolation.* ISPRS Int. J. Geo-Inf., 7, 300, 15 pp., doi: 10.3390/ijgi7080300.

Schellekens J., Brolsma R.J., Dahm R.J., Donchyts G.V. and Winsemius H.C.; 2014: *Rapid setup of hydrological and hydraulic models using OpenStreetMap and the SRTM derived digital elevation model*. Environ. Modell. Softw., 61, 98-105.

Sefercik U.G., Yastikli N. and Dana I.; 2014: *DEM extraction in urban areas using high-resolution TerraSAR-X imagery*. J. Indian Soc. Remote Sens., 42, 279-290.

Shabou A., Baselice F. and Ferraioli G.; 2012: *Urban digital elevation model reconstruction using very high resolution multichannel InSAR data.* IEEE Trans. Geosci. Remote Sens., 50, 4748-4758.

Śledź S. and Ewertowski M.W.; 2022: *Evaluation of the influence of processing parameters in structure-from-motion software on the quality of digital elevation models and orthomosaics in the context of studies on Earth surface dynamics.* Remote Sens., 14, 1312, 15 pp., doi: 10.3390/rs14061312.

Tayebi M., Tayebi M.H. and Sameni A.; 2017: *Soil erosion risk assessment using GIS and CORINE model: a case study from western Shiraz, Iran.* Arch. Agron. Soil Sci., 63, 1163-1175.

Torun A.T.; 2022: *Accuracy comparison of digital elevation models produced from ascending and descending orbits TerraSAR-X data*. Çukurova Üniversitesi Mühendislik Fakültesi Dergisi, 37, 367-376, in Turkish.

Torun A.T. and Orhan O.; 2021. *Investigation of temporal baseline effect on DEMs derived from COSMO Sky-Med data.* Int. J. Eng. Geosci., 6, 157-164.

Uuemaa E., Ahi S., Montibeller B., Muru M. and Kmoch A.; 2020: *Vertical accuracy of freely available global digital elevation models (ASTER, AW3D30, MERIT, TanDEM-X, SRTM, and NASADEM).* Remote Sens., 12, 3482, 23 pp., doi: 10.3390/rs12213482.

Wu W., Fan Y., Wang Z. and Liu H.; 2008: *Assessing effects of digital elevation model resolutions on soil-landscape correlations in a hilly area.* Agric. Ecosyst. Environ., 126, 209-216.

Yildiz S., Akyürek Z. and Aydın A.; 2018: *Accuracy assessment of digital elevation model (DEM) derived from 1/25000 scale standard topographic maps*. In: Proc. VII. Uzaktan Algılama Ve CBS Sempozyumu, Eskişehir, Turkey, 1 p., doi: 10.15659/uzalcbs2018.6126.

Zhang G., Wang S., Chen Z., Liu Y., Xu Z. and Zhao R.; 2023: *Landslide susceptibility evaluation integrating weight of evidence model and InSAR results, west of Hubei Province, China.* Egypt. J. Remote Sens. Space Sci., 26, 95-106.

Zhang W. and Montgomery D.R.; 1994: *Digital elevation model grid size, landscape representation, and hydrologic simulations.* Water Resour. Res., 30, 1019-1028.

Corresponding author: Hasan Bilgehan Makineci
Geomatics Engineering Department, Konya Technical University
Yeni Istanbul Street, Selçuklu, Konya, Turkey
Phone: +90 332 205 1640; e-mail: hbmakineci@ktun.edu.tr